Transmission of digitally encoded speech at 1.2 Kbaud for PCN

L. Hanzo, MSc, PhD
R. Salami, MSc, PhD
Prof. R. Steele, DSc, MIEE, MIEEE
P.M. Fortune, BSc, PhD

Indexing terms: Channel coding, Speech coding, Modulation, Microcellular digital mobile networks, PCN

Abstract: The transmission of digitally encoded speech at 1.2 Kbaud for mobile personal communication networks (PCN) is investigated both analytically and by computer simulations. Speech was encoded at 4.8 Kbit/s using a low complexity transformed binary pulse excited LPC codec. A 64-level QAM modem was used having three subchannels that operated with different BERs. The sensitivity of the encoded speech bits to transmission errors was identified, and the bits classified into three groups. Each group was then individually coded by BCH codecs of differing power. The output of the BCH coders were Gray coded onto the three QAM channels. By this arrangement the protection given to the speech bits was dependent on their vulnerability. The six-bit QAM symbols were transmitted at 1.2 Kbaud over Rayleigh fading channels with pedestrian mobiles travelling up to 4 mile/h. For microcells using a propagation frequency of 1.9 GHz and operating with channel SNRs in excess of 26 dB we achieved good communications quality speech when second-order diversity and AGC were used.

1 Introduction

Personal communication networks (PCN) of the near future will operate with relatively high traffic densities to service the plethora of low-cost, low-power-consumption, lightweight handheld portables that are expected to be deployed. Fortunately these high densities can be provided using microcellular digital mobile radio networks, where the dramatically reduced transmitted power and small cell size render far-field reflections negligible, keeping the excess delay spread to a minimum. The frequency re-use distances are inherently small, yielding high traffic densities and favourable propagation characteristics.

Following the philosophy of the second-generation Japanese digital mobile radio system, where no channel equaliser is deployed in the diversity-assisted two bits per symbol quadrature phase shift keying (QPSK) modem [1], we further reduce the signalling rate by using six bits per symbol transmissions. This in turn extends the signalling interval to proportionately mitigate the effects of channel dispersion. Consequently, for true microcells there is no need for channel equalisers and six bits per symbol multilevel modulation schemes combined with diversity, automatic gain control (AGC) and carefully matched embedded low-complexity forward error correction codecs offer spectrally efficient mobile radio links where, thanks to the low transmitted power, the amplifier linearity is less of a problem. To control spectral spillage into adjacent channels either spectrally less efficient moderately rolled-off filtering must be accepted as a penalty, or in more complex systems the equaliser must be designed to cope with the additional intersymbol interference introduced by sharp filters. In our scheme we favour the first, less efficient, low-complexity approach and use no equaliser.

In a companion paper [2] we reported that a 16-level quadrature amplitude modulation (16-QAM) scheme, combined with either low-complexity Bose-Chaudhuri-Hocquenghem (BCH) codecs, or the more powerful Reed-Solomon (RS) codes [3] can guarantee the necessary integrity for the transmission of sub-band coded (SBC) speech, with the proviso of using automatic gain control (AGC) and phase locking. For channel signal-to-noise ratios (SNRs) in excess of 22 dB, and for various mobile speeds, near toll quality speech communication was achieved. The systems's robustness was dramatically improved when second-order switched diversity and speech post-enhancement methods were deployed. The transmission rate was 5 Kbaud. Pursuing a similar approach, but using a transformed binary excited codec [4], allowed us to reduce the signalling rate to 2.1 Kbaud [5].

Encouraged by our findings, we now embark on the investigation of a combined, low-complexity speech coding, channel coding and modulation scheme having excellent spectral efficiency, while maintaining all the other desirable attributes essential for personal communications. We commence by investigating the suitability of a coherent 64-QAM scheme over both Gaussian and Rayleigh-fading channels using theory and simulations. We then propose a low-complexity fade-tracking AGC to significantly increase the 64-QAM performance and show that second-order switched diversity results in a performance similar to that achieved over Gaussian channels. Computationally-efficient binary BCH codes are

Paper 8802I (E5, E8), first received 15th March and in revised form 12th November 1991

The authors are with the Department of Electronics and Computer Science, University of Southampton, Southampton SO9 5NH, United Kingdom

deployed to remove the residual errors after AGC and diversity reception. The speech codec is a highly efficient, good communications quality 4.8 Kbit/s transformed binary pulse-excited (TBPE) codec [4], having the quality of the code-excited linear predictive (CELP) codec [10], while offering a direct excitation computation procedure. Three variations of the combined system are described, evaluated and compared in terms of objective and subjective performance. Our best candidate system fulfills the main requirements of the PCNs.

2 64-level QAM

Each constellation point in 64-level QAM systems is represented by a unique six-bit symbol, which is Gray-coded to minimise the decoded error probability, Fig. 1. The

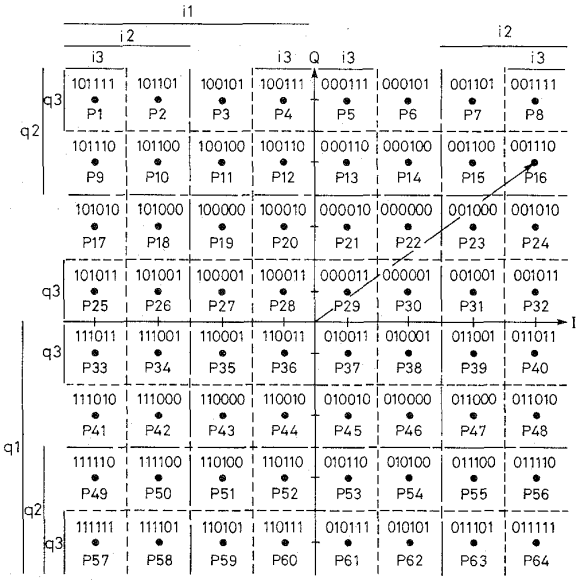

Fig. 1 *64-level QAM constellation*
—·— C2 subchannel decision boundaries
------- C3 subchannel decision boundaries
d = coordinate spacing

complex phasors of the constellation are decomposed into the eight-level in-phase (I) and quadrature-phase (Q) amplitude modulated (AM) signals. The amplitudes $7d$, $5d$, $3d$, d, $-d$, $-3d$, $-5d$ and $-7d$ of the I and Q AM signals are assigned the three-bit Gray codes 011, 010, 000, 001, 101, 100, 110 and 111, respectively. The three I and Q bits are denoted by i_1, i_2, i_3 and q_1, q_2, q_3, respectively. These bits are interleaved to give a 6-bit QAM symbol represented by $i_1, q_1, i_2, q_2, i_3, q_3$.

The 64-level QAM phasors are transmitted over the mobile radio channel, where they inevitably become corrupted. They are demodulated using the decision boundaries shown in Fig. 1. Observe that the construction of the signal constellation is similar to that of a Karnaugh table, where in the left half plane of the coordinate axis i_1 is always logical 1 and in the bottom half plane q_1 is logical 1, etc. The bits $i_1, q_1, i_2, q_2, i_3, q_3, i_4, q_4$ are recovered according to

$$\begin{aligned} &\text{if } I, Q \geq 0 \quad \text{then } i_1, q_1 = 0 \\ &\text{if } I, Q < 0 \quad \text{then } i_1, q_1 = 1 \end{aligned} \tag{1}$$

for the most significant bits, and

$$\begin{aligned} &\text{if } I, Q \geq 4d \quad \text{then } i_2, q_2 = 1 \\ &\text{if } -4d \leq I, Q < 4d \quad \text{then } i_2, q_2 = 0 \\ &\text{if } -4d > I, Q \quad \text{then } i_2, q_2 = 1 \end{aligned} \tag{2}$$

for the next most signficant bits, and finally for the least significant bits

$$\begin{aligned} &\text{if } I, Q \geq 6d \quad \text{then } i_3, q_3 = 1 \\ &\text{if } 2d \leq I, Q < 6d \quad \text{then } i_3, q_3 = 0 \\ &\text{if } -2d \leq I, Q < 2d \quad \text{then } i_3, q_3 = 1 \\ &\text{if } -6d \leq I, Q < -2d \quad \text{then } i_3, q_3 = 0 \\ &\text{if } -6d > I, Q \quad \text{then } i_3, q_3 = 1 \end{aligned} \tag{3}$$

Observe that the position of the bits in the six-bit QAM symbol has a profound effect on their error probabilities. In case of the i_1, q_1 bits, for example, the phasor can be at a distance d, $3d$, $5d$ or $7d$ from the decision boundary represented by the coordinate axis. Therefore, their average 'protection distance' is $16d/4 = 4d$. Fig. 1 reveals that this average protection distance for the i_2, q_2 bits is $2d$, while for the i_3, q_3 bits it is d. The bits (i_1, q_1), (i_2, q_2) and (i_3, q_3) may be viewed as three subchannels each having different integrities. These channels will be referred to as $C1$, $C2$ and $C3$, respectively.

2.1 64-QAM performance for transmission over Gaussian channels

Assume that an independent random data sequence is conveyed to each of the $C1$, $C2$ and $C3$ subchannels, and that perfect coherent detection is carried out at the receiver using eqns. 1 to 3. Let us determine the bit error rate (BER) performance of the I component, as the Q component being in quadrature will support data that is subjected to the same BER. The channel will be assumed to be an additive white Gaussian noise (AWGN) one.

Consider first the $C3$ subchannel (i_3, q_3) with its decision boundaries of $-6d$, $-2d$, $2d$ and $6d$. Each phasor has a different error probability, depending on its position in the constellation of Fig. 1. The bit i_3 of phasor P_5 (a logical 1) will, for example, be corrupted if a noise sample with larger amplitude than d is added to it when the decoded phasor is P_6, but when it is carried by a noise vector having larger than $5d$ amplitude over the $C3$ decision boundary at $6d$, the decision becomes error-free again, although the decoded phasor is erroneously considered to be P_8. In the negative direction there is no corruption until the noise amplitude reaches $-3d$ (phasor P_3). For noise vectors having amplitudes between $-3d$ and $-7d$ there are erroneous decisions, but once the $-6d$ decision boundary is exceeded, i.e. the negative noise value is larger than $-7d$, the received sample falls into the error-free domain again although the decoded phasor is P_1. The i_3 bit error probability of the P_5 phasor is given by the following summation of Q-functions:

$$P_{e5} = Q\left[\frac{d}{\sqrt{(N_0/2)}}\right] + Q\left[\frac{3d}{\sqrt{(N_0/2)}}\right] - Q\left[\frac{5d}{\sqrt{(N_0/2)}}\right] - Q\left[\frac{7d}{\sqrt{(N_0/2)}}\right] \tag{4}$$

where N_0 denotes the one-sided Gaussian noise spectral density. After averaging the powers of the individual phasors $P_1, \ldots, P_{64}$ the average symbol energy for 64-QAM is found to be $E = 42d^2$. Substituting $d = \sqrt{(E/42)}$ into eqn. 4, and introducing the average signal-to-noise ratio (SNR) $\gamma = E/N_0$, we get

$$P_{e5} = Q\left[\sqrt{\frac{\gamma}{21}}\right] + Q\left[3\sqrt{\frac{\gamma}{21}}\right] - Q\left[5\sqrt{\frac{\gamma}{21}}\right] - Q\left[7\sqrt{\frac{\gamma}{21}}\right] \quad (5)$$

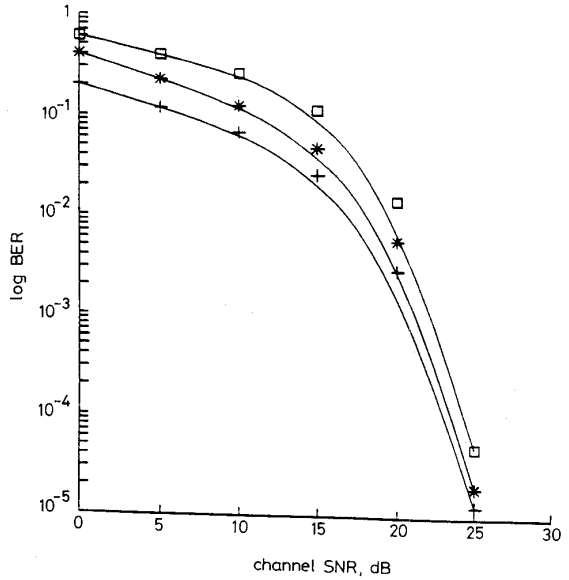

Fig. 2 *C1, C2 and C2 BER via AWGN channels against SNR*

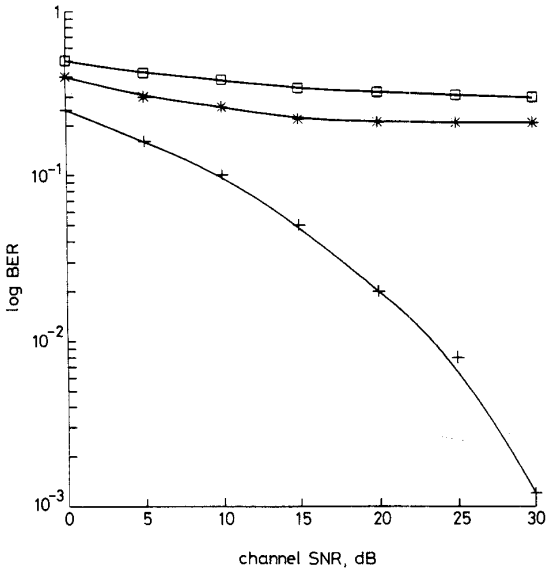

Fig. 3 *C1, C2 and C3 BER via Rayleigh-fading channels against SNR*

For the phasor P_8 the situation is different, as its $C3$ bit i_3 is not corrupted by positive noise samples of arbitrary large amplitudes. For negative noise levels it cycles in and out of error as the noise increases past $-d$, $-5d$, $-9d$ and $-13d$, as seen in Fig. 1. Therefore the associated error probability is

$$P_{e8} = Q\left[\sqrt{\frac{\gamma}{21}}\right] + Q\left[9\sqrt{\frac{\gamma}{21}}\right] - Q\left[5\sqrt{\frac{\gamma}{21}}\right] - Q\left[13\sqrt{\frac{\gamma}{21}}\right] \quad (6)$$

Following a similar argument the error probability P_{e6} of the i_3 bit of phasor P_6 is

$$P_{e6} = Q\left[\sqrt{\frac{\gamma}{21}}\right] + Q\left[3\sqrt{\frac{\gamma}{21}}\right] - Q\left[5\sqrt{\frac{\gamma}{21}}\right] + Q\left[9\sqrt{\frac{\gamma}{21}}\right] \quad (7)$$

while

$$P_{e7} = Q\left[\frac{\gamma}{21}\right] + Q\left[3\sqrt{\frac{\gamma}{21}}\right] - Q\left[7\sqrt{\frac{\gamma}{21}}\right] + Q\left[11\sqrt{\frac{\gamma}{21}}\right] \quad (8)$$

The error probabilities P_{e1}, P_{e2}, P_{e3}, P_{e4} are equivalent to those given by P_{e8}, P_{e7}, P_{e6}, P_{e5}, respectively, and the same holds for all corresponding phasors in the columns of the phasor diagram of Fig. 1. Furthermore, the q_3 bit error probability is identical to that of i_3, if independent random sequences are transmitted. Averaging the $C3$ bit error probabilities yields:

$$P_{C3}(\gamma) = Q\left[\sqrt{\frac{\gamma}{21}}\right] + \tfrac{3}{4}Q\left[3\sqrt{\frac{\gamma}{21}}\right] - \tfrac{3}{4}Q\left[5\sqrt{\frac{\gamma}{21}}\right] - \tfrac{1}{2}Q\left[7\sqrt{\frac{\gamma}{21}}\right] - \tfrac{1}{4}Q\left[9\sqrt{\frac{\gamma}{21}}\right] - \tfrac{1}{4}Q\left[11\sqrt{\frac{\gamma}{21}}\right] - \tfrac{1}{4}Q\left[13\sqrt{\frac{\gamma}{21}}\right] \quad (9)$$

The last three terms in eqn. 9 represent extremely unlikely events as the Gaussian noise sample must exceed the $9d$ protection distance of the best protected $C1$ bit. Consequently we neglect these terms.

Applying similar arguments to those used in the formulation of $P_{C3}(\gamma)$, we have the bit error probabilities for $C2$ and $C1$ as

$$P_{C2}(\gamma) = \tfrac{1}{2}Q\left[\sqrt{\frac{\gamma}{21}}\right] + \tfrac{1}{2}Q\left[\sqrt{\frac{3\gamma}{21}}\right] + \tfrac{1}{4}Q\left[\sqrt{\frac{5\gamma}{21}}\right] + \tfrac{1}{4}Q\left[\sqrt{\frac{7\gamma}{21}}\right] \quad (10)$$

and

$$P_{C1}(\gamma) = \tfrac{1}{4}Q\left[\sqrt{\frac{\gamma}{21}}\right] + \tfrac{1}{4}Q\left[\sqrt{\frac{3\gamma}{21}}\right] + \tfrac{1}{4}Q\left[\sqrt{\frac{5\gamma}{21}}\right] + \tfrac{1}{4}Q\left[\frac{7\gamma}{21}\right] \quad (11)$$

The P_{C1}, P_{C2} and P_{C3} error probability curves evaluated using eqns. 9–11 are displayed in Fig. 2. Our simulation

results differed by less than a dB from these curves. Observe the consistent bit error rate advantage obtained using the $C1$ subchannel. All subchannels have BERs $< 10^{-3}$ for SNR values in excess of 23 dB. They are therefore suitable for digitised speech transmission. Notice that for SNRs above 23 dB there is only a modest BER advantage in using the $C1$ subchannel.

2.2 64-QAM performance via Rayleigh-fading channels

The situation is far more complex over Rayleigh-fading channels because the effect of fading on each phasor and on its decision boundary has to be considered individually for the $C2$ and $C3$ subchannels. The analytically derived $C1$, $C2$ and $C3$ error probabilities for Rayleigh channels are given by eqns. 20, 25 and 30 of Section 10. The numerical evaluation of these equations yields the curves displayed in Fig. 3. Simulation results agreed with these curves to within a fraction of a dB. Observe that the $C1$ BER sharply decreases with increasing channel SNRs, and above 30 dB it falls below 10^{-3}, a value suitable for good communications quality speech. The $C2$ and $C3$ BER performances show little improvement with increasing channel SNR and are unsuitable for reliable speech communication. By using a fade-compensating automatic gain control (AGC) the $C2$ and $C3$ BERs can be decreased to a value that can be combatted by forward error correction (FEC) techniques.

3 Fade-tracking AGC for 64-QAM

PCN is particularly concerned with mobile stations carried by pedestrians. The received signal envelopes are subjected to slow fading rates. Fig. 4 shows a Rayleigh-

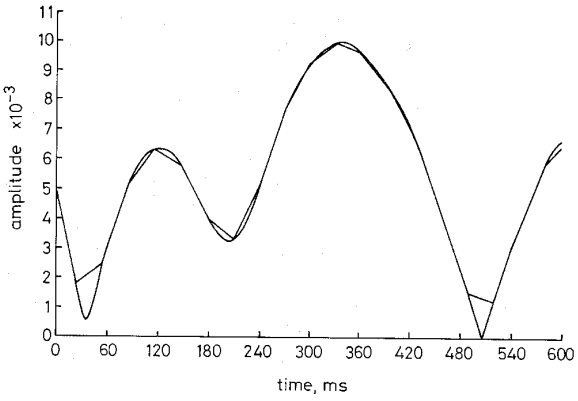

Fig. 4 *Operation of AGC fade-tracking at 1.9 GHz, $k = 30$ and 2 mile/h*

fading envelope for a mobile station travelling at 1 mile/h, a situation when a pedestrian MS is walking slowly while making a phone call. Notice that although Rician fading will often occur we are using the worst case scenario of Rayleigh fading.

Imagine that every kth transmitted 64-QAM phasor is to be, for example, P_8 in Fig. 1. If the absolute value of this 'channel sounding phasor' is different from its expected value, as is usually the case, this is attributed to the effect of channel fading. The ratio of the expected and received P_8 values defines a gain factor used in our fade-tracking AGC. We arrange for the previously received k phasors to be stored in a buffer for fade compensation, the first of which is the previous 'channel sounding phasor'. Using the previous and present received channel sounding phasors P_8 having absolute values R_1 and R_2, respectively, we compute their difference and divide by k to derive the fade compensation stepsize: $s = (R_1 - R_2)/k$. This step size s is then used between two channel sounding phasors to linearly approximate the fading envelope. The process is shown in Fig. 4, where for demonstration, a 64-QAM transmission rate of 1 Kbaud resulting in 30 transmitted phasors in each 30 ms interval, and a channel sounding interval of $k = 30$ is assumed. Due to these particular parameters the Rayleigh-fading envelope of Fig. 4 is linearly approximated by the fade-tracking AGC, as seen in Fig. 4. The fade tracking AGC is a good approximation to the envelope at high signal levels, but 'cuts corners' at deep fades resulting in burst errors. These errors are combatted using diversity and FEC techniques.

The selection of the channel sounding parameter k is based on two contradictory factors. The lower the value of k, the better is the linear approximation to the Rayleigh envelope, but the higher is the bit rate due to the transmission of more channel sounding phasors. In addition, the effect of channel noise on the sounding phasors, and hence on AGC performance, must be considered. To determine k we found the $C1$, $C2$ and $C3$ BERs as a function of channel SNR for transmissions over Rayleigh-fading channels. Although the parameter k was varied between 5 and 30 we soon truncated our investigation to the values of $k = 10$ and $k = 20$. We emphasise that we are primarily interested in the system performance for mobiles operating at walking speeds, say 1 to 4 mile/h. Inspection of Fig. 4 reveals that with the increase of mobile speed the fading rate is also linearly increased, which results in gradually deteriorated fade-tracking ability, namely increased BER. The $C1$, $C2$ and $C3$ BERs versus channel SNR curves for fade-tracking AGC with sounding periods of $k = 10$ and $k = 20$, and for mobile speeds of $v = 2$ mile/h and 4 mile/h are shown in Figs. 5, 6 and 7, respectively. For all the $C1$, $C2$ and $C3$ sub-

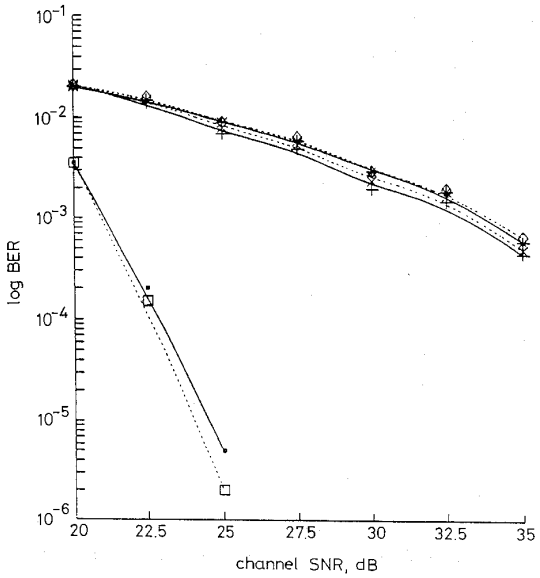

Fig. 5 *64-QAM C1 BER with fade-tracking AGC*

- AWGN, 10
- 2 mile/h, 10
- 4 mile/h, 10
- AWGN, 20
- 2 mile/h, 20
- 4 mile/h, 20

classes, and for both mobile speeds, a consistent BER improvement was achieved when $k = 10$. The transmission overhead was only 5% compared to when $k = 20$

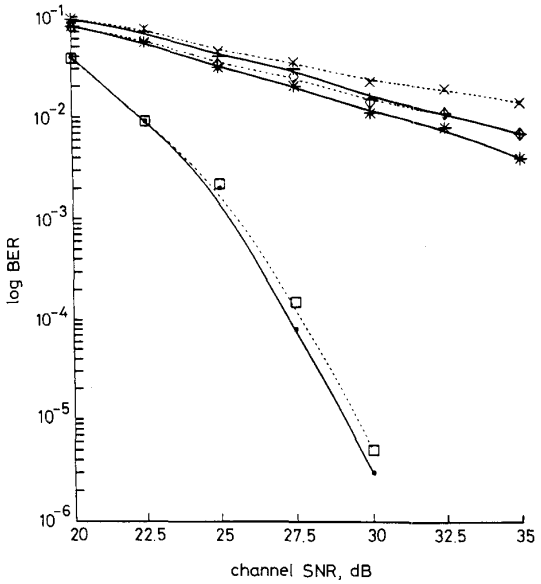

Fig. 6 *64-QAM C2 BER with fade-tracking AGC*
AWGN, 10
2 mile/h, 10
4 mile/h, 10
AWGN, 20
2 mile/h, 20
4 mile/h, 20

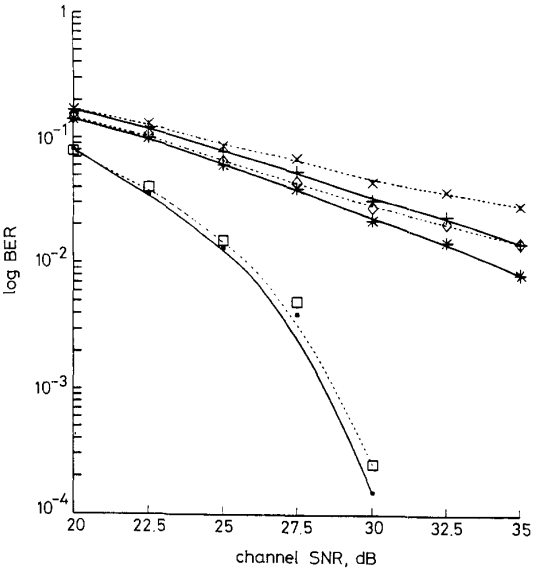

Fig. 7 *64-QAM C3 BER with fade-tracking AGC*
AWGN, 10
2 mile/h, 10
4 mile/h, 10
AWGN, 20
2 mile/h, 20
4 mile/h, 20

and we therefore opted for $k = 10$. Notice that there was a significant reduction in the BERs of $C2$ and $C3$ as compared to that with no AGC depicted in Fig. 3. This was achieved at the price of only a 10% transmission overhead (the sounding phasor) and a negligible complexity penalty was incurred. For channel SNRs in excess of 30 dB, which may be realisable in the microcells of a PCN, the BER of all subchannels was sufficiently low to be combatted by practical, low-complexity FEC methods.

The order of integrity of the subchannels was also preserved, which we will exploit in our jointly optimised system. In AWGN channels the 64-QAM BER performance was slightly degraded by the fade-tracking AGC as there was no envelope fading, and the noisy received channel sounding phasors slightly falsified the amplitudes of the information phasors. Nonetheless, the FEC codes adopted must be able to cope with the more hostile Rayleigh channel.

4 Switched diversity for 64-QAM

In a previous paper [2] we found that switched diversity improved the BER performance of a 16-QAM system by using a received signal-energy controlled AGC. Encouraged by this, we introduced diversity to improve our 64-QAM system, where each of the received signals in our simulation were transmitted over a different, independent Rayleigh-fading channel. Each of the received signals was assigned a separate fade-tracking AGC, and in each channel sounding interval the channel exhibiting the highest average energy was selected for demodulation. As the AGC used energy averaging over k samples the total system delay was increased accordingly.

Our results for the $C1$, $C2$ and $C3$ subchannels when diversity reception of order $DIV = 1, \ldots, 5$ was used and the speed of the mobile was 2 mile/h are depicted in Fig. 8, 9 and 10, respectively. When the channel SNR was in

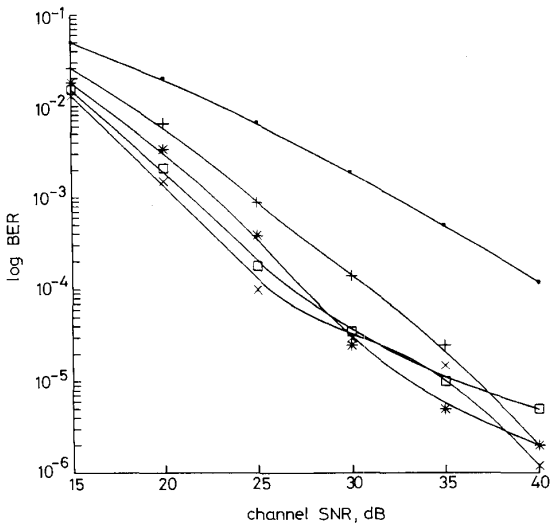

Fig. 8 *C1 BER at 2 mile/h with various orders of diversity*
DIV = 1
DIV = 2
DIV = 3
DIV = 4
DIV = 5

excess of 25 dB and second-order diversity ($DIV = 2$) used, there was nearly an order of magnitude improvement in the BER for all three subclasses. Increasing the order of diversity from 3 to 5 yielded progressively smaller reductions in BER and for an increasing amount of receiver complexity. For high SNR values a residual BER is observed for all diversity orders, because the receiver performance is dominated by the AGC's deficiency of 'cutting corners' at deep fades, as seen in Fig. 4,

which is also the reason for the unexpected worse performance of high-order diversity schemes. In conclusion therefore, we opted for second-order diversity reception.

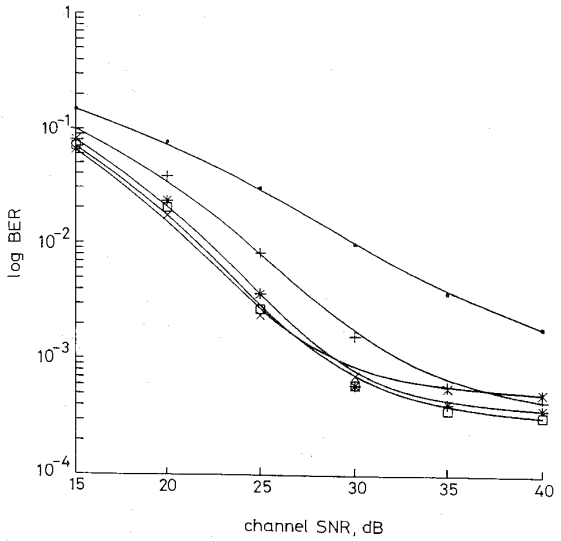

Fig. 9 *C2 BER at 2 mile/h with various orders of diversity*
—■— DIV = 1
—+— DIV = 2
—*— DIV = 3
—□— DIV = 4
—×— DIV = 5

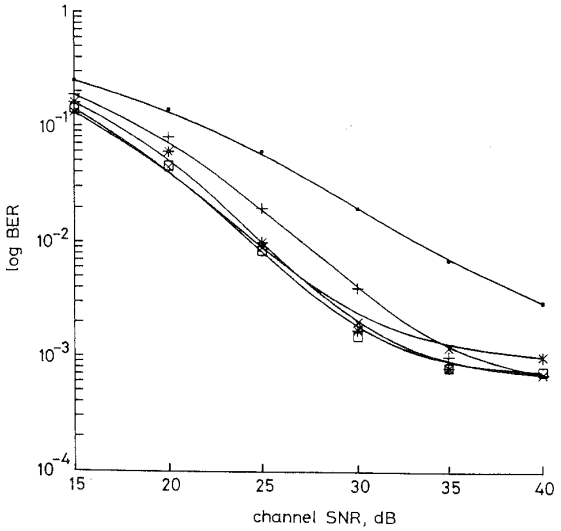

Fig. 10 *C3 BER at 2 mile/h with various orders of diversity*
—■— DIV = 1
—+— DIV = 2
—*— DIV = 3
—□— DIV = 4
—×— DIV = 5

5 Selection of FEC codes

Convolutional codes [6] are powerful over memoryless AWGN channels, but over fading channels they require the interleaving depth to be very high if the bursty channel is to appear as a near-memoryless one. This delay is, in general, unacceptable in speech communications. Furthermore, CCs require soft-decision decoding if they are to be effective. Unfortunately, the high number of constellation points in 64-QAM results in great complexity when soft decisions are to be used, a factor that renders it unacceptable if we are to achieve a low-consumption, lightweight hand-held personal communicator. Although the BER performance of CCs can be improved by increasing the code constraint length, this approach again results in a complexity penalty. Lastly, we note that CCs have no error detection capability, a most serious disadvantage in mobile communications.

By contrast, Reed-Solomon block codes [7] possess maximum minimum distance properties making them powerful in correcting errors with arbitrary distributions. High blocklengths [8] tend to transform a fading channel into a near memoryless one, at the expense of high complexity and delay. Fortunately, a similar performance can be achieved by using shorter low-complexity block codes combined with interleavers. Similar BER performances can be obtained using binary Bose-Chaudhuri-Hocquenghem codes [2], having lower decoding complexities than RS codes. Both BCH and RS codes have good error correcting powers and error detection capabilities, important advantages over CCs. The error detection capability may be used in speech post-enhancement methods [8], or to initiate handover between base stations [9].

From these arguments we favour binary BCH codes for microcellular environments where low-complexity, low-consumption, lightweight hand-held mobile phones are used. The BER performance of a set of various BCH codes with a moderate 63 bit wordlength has been evaluated [2]. The preselected codes are the BCH(63, 57, 1), BCH(63, 51, 2), BCH(63, 45, 3), BCH(63, 39, 4), BCH(63, 36, 5), BCH(63, 30, 6), BCH(63, 24, 7), where 63 is the encoded wordlength, the second parameter represents the number of bits to be encoded and the third parameter is the number of bits correctable by the specific code. We propose to use codes from this set after we have formulated the specific bit-packing and bit-protection requirements of the various 64-QAM subchannels, as well as those of the specific speech bits. In other words, we use the BCH codecs to generate 64-QAM superchannels having appropriate BER performances for the transmission of the particular speech bit classes possessing various BER sensitivities.

6 The 4.8 Kbit/s transformed binary pulse-excited speech codec

To provide extremely high traffic density we propose a low-bit-rate, low-complexity transformed binary pulse excited (TBPE) speech codec, delivering high communications quality speech at 4.8 kbit/s [4]. The TBPE codec provides the speech quality of the original code-excited linear predictive (CELP) codec but at greatly reduced complexity.

6.1 Excitation optimisation in TBPE codecs

Regularly spaced Gaussian excitation vectors of dimension M with a pulse-spacing of D excite the synthesis filter formed as the concatenation of the long-term prediction (LTP) and the LPC synthesis filters. In the CELP codecs the optimum codebook entry is determined by evaluating the synthetic speech due to each codebook vector, i.e. typically 1024 times, whereas in TBPE the optimum excitation vector minimising the weighted mean squared error between the original and synthetic speech is derived in one direct computation step. The sparse Gaussian excitation vector is

$$\boldsymbol{c} = A\boldsymbol{b} \tag{12}$$

where the binary vector $\boldsymbol{b}$ has M elements of ± 1, while the $M \times M$ matrix A represents an orthogonal transformation. Owing to the orthogonality of A, the binary excitation pulses of $\boldsymbol{b}$ are transformed into independent, unit variance Gaussian components of $\boldsymbol{c}$. The set of 2^M binary excitation vectors gives rise to 2^M Gaussian vectors of the original CELP codec. For CELP codecs, the weighted mean squared error [10] is

$$E_w = \sum_{n=0}^{N} x^2(n) - \frac{\left[\sum_{i=1}^{M} \Psi(i)c(i)\right]^2}{\sum_{i=1}^{M}\sum_{j=1}^{M} c(i)c(j)\Phi(i,j)} \quad (13)$$

where $x(n)$ represents the weighted original speech with the filter memories removed from it, and

$$\Phi(i,j) = \sum_{n=1}^{M} h(n-i)h(n-j)$$

are the covariance of the impulse response $h(n)$ of the cascaded filter combination of the synthesis and error weighting filters. The excitation samples $c(i)$, $c(j)$ are the components of the Gaussian vector $\boldsymbol{c}$, and $\Psi(n) = x(n) * h(-n)$ is the crosscorrelation of $x(n)$ and $h(n)$. The expression of eqn. 13 has to be minimised over the Gaussian codebook in CELP codecs.

The direct excitation of the TBPE codec accrues from the matrix representation of eqn. 13 using eqn. 12, namely

$$E = \boldsymbol{x}^T\boldsymbol{x} - \frac{(\boldsymbol{\Psi}^T A\boldsymbol{b})^2}{\boldsymbol{b}^T \mathrm{A}^T \Phi \mathrm{A}\boldsymbol{b}} \quad (14)$$

The denominator in eqn. 14 is nearly constant over the entire codebook and hence plays practically no role in the excitation optimisation. This is because the autocorrelation matrix Φ is strongly diagonal, since the impulse response $h(n)$ decays sharply. Owing to the orthogonality of A, we have $\mathrm{A}^T\mathrm{A} = \mathrm{I}$, where I is the identity matrix, causing the denominator to be constant.

Closer scrutiny of eqn. 14 reveals that its second term reaches its maximum if the binary vector element $b(i) = -1$, whenever the vector element $\boldsymbol{\Psi}^T\mathrm{A}$ is negative, and *vice-versa*, i.e. $b(i) = +1$ if $\boldsymbol{\Psi}^T\mathrm{A}$ is positive. The numerator of eqn. 14 is then constituted by exclusively positive terms, i.e. it is maximum, and the weighted mean squared error is minimum. The optimum Gaussian excitation is computed from eqn. 12 in both the encoder and decoder. Only the M-bit index representing the optimum binary excitation vector $\boldsymbol{b}$ has to be transmitted. The evaluation of the vectors $\boldsymbol{\Psi}^T\mathrm{A}$ and $\boldsymbol{c} = \mathrm{A}\boldsymbol{b}$ requires a mere $2M^2$ number of multiplications/additions, which gives typically five combined operations per output speech sample, a value 400 times lower than the complexity of the equivalent quality CELP codec.

The bit allocation of our TBPE codec is summarised in Table 1. The spectral envelope is represented by ten line spectrum frequencies (LSFs) which are scalar quantised using 36 bits. The 30 ms long speech frames having 240 samples are divided into four 7.5 ms subsegments having 60 samples. The subsegment excitation vectors $\boldsymbol{b}$ have 12 transformed duo-binary samples with a pulse spacing of $D = 5$. The LTP delays (LTPD) are quantised with seven bits in odd and five bits in even indexed subsegments, while the LTP gain (LTPG) is quantised with three bits. The excitation gain (EG) factor is encoded with four bits, while the grid position (GP) of candidate excitation sequences by two bits. A total of 28 or 26 bits per subsegment is used for quantisation, which yields $36 + 2 \times 28 + 2 \times 26 = 144$ bits per 30 ms, i.e. a bitrate of 4.8 Kbit/s.

Table 1: Bit allocation of 4.8 kbit/s TBPE codec

Parameter	Bit number
10 LSFs	36
LTPD	2 × 7 + 2 × 5
LTPG	4 × 3
GP	4 × 2
EG	4 × 4
Excitation	4 × 12
Total	144

6.2 *Bit sensitivity analysis of the 4.8 Kbit/s TBPE speech codec*

The effect of the sensitivities of the TBPE bits to transmission errors was investigated in terms of segmental signal-to-noise ratio (SEG-SNR) and the cepstrum distance measure [11, 12], defined as

$$CD \approx \sqrt{\left([C_x(0) - C_y(0)]^2 + 2\sum_{i=1}^{3p}[C_x(i) - C_y(i)]^2\right)} \quad (15)$$

where $C_x(i)$ and $C_y(i)$ represent the input and output speech cepstral coefficients computed from the LPC coefficients of the input and output speech, and $p = 10$ is the order of the all-pole LPC analysis filter.

In our bit sensitivity investigations we systematically corrupted each bit of a 144 bit TBPE frame and evaluated the SEG-SNR and *CD* degradation. Our results are depicted for the first 63 bits of a TBPE frame in Fig. 11.

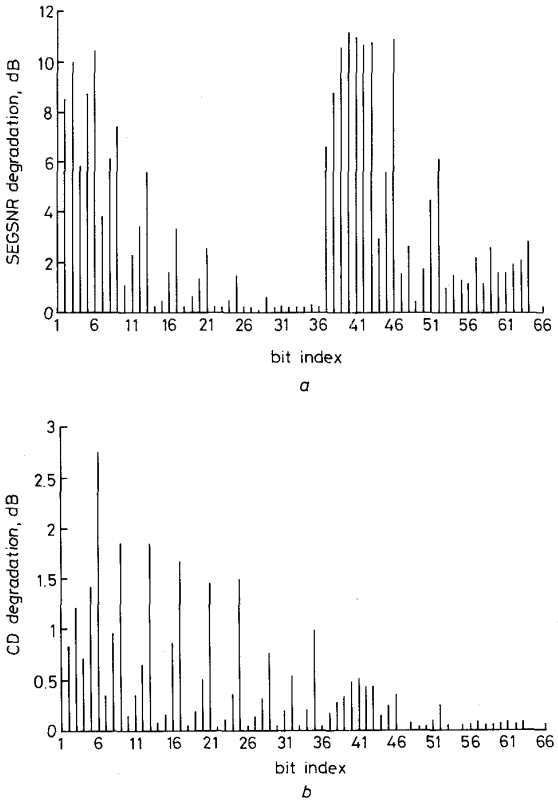

Fig. 11 *Bit sensitivities for the 4.8 Kbit/s codec*
a in terms of SEG-SNR degradation
b in terms of CD degradation

Table 2: Sensitivity figures for the 4.8 Kbit/s TBPE codec

Bit no. in frame	Bit index in frame	Sensitivity figure	Bit no. in frame	Bit index in frame	Sensitivity figure
1	6	8	36	57	76
2	9	14	37	10	79
3	5	16	38	28	80
4	3	16	39	19	80
5	41	19	40	61	80
6	40	20	41	59	82
7	13	21	42	62	84
8	2	23	43	15	85
9	43	24	44	60	88
10	8	25	45	34	89
11	46	25	46	50	91
12	42	26	47	31	92
13	17	27	48	55	95
14	39	31	49	27	95
15	4	31	50	23	97
16	21	32	51	14	97
17	12	37	52	47	98
18	38	38	53	58	102
19	25	43	54	54	103
20	16	44	55	53	105
21	52	45	56	56	105
22	7	45	57	18	105
23	1	45	58	33	108
24	37	48	59	49	109
25	45	49	60	26	109
26	11	55	61	30	110
27	20	58	62	22	119
28	51	60	63	36	125
29	29	60			
30	35	60			
31	44	63			
32	32	68			
33	48	69			
34	24	71			
35	63	76			

We recall from Table 1 that the first 36 bits represent the 10 LSFs describing the speech spectral envelope. The SEG-SNR degradations shown in Fig. 11*a* indicate the most severe waveform distortions for the first 10 bits describing the first 2–3 LSFs. The *CD* degradation, however, was quite severe for all LSFs, particularly for the most significant bits (MSBs) of the individual parameters. This was confirmed by our informal subjective tests. Whenever possible, all LSF bits should be protected against corruption.

The situation is practically reversed for the rest of the 144 bits in the TBPE frame, which represent the LTPD, LTPG, GP, EG and excitation parameters for the subsegments. We highlight our findings for the case of the first 27-bit subsegment only, as the other subsegments have identical behaviours. Bits 37–43 represent the LTP delays and bits 44–47 the LTP gains. Their errors are more significant in terms of SEG-SNR than in *CD*, as demonstrated by Fig. 11. This is because the LTPD and LTPG parameters describe the spectral fine structure and do not seriously influence the spectral envelope, although they seriously degrade the recovered waveform. As the TBPE codec is a stochastic codec with random excitation patterns, the bits 48–63 assigned to the excitations and their gains are not particularly vulnerable to transmission errors. This is because the redundancy in the signal is removed by the long-term and short-term predictors. Furthermore, the TBPE codec exhibits exceptional inherent excitation robustness, as the influence of a channel error in the excitation diminishes after the orthogonal transformation $\boldsymbol{c} = \mathrm{A}\boldsymbol{b}$. In conventional CELP codecs this is not the case, as a codebook address error causes the decoder to select a different excitation pattern from its codebook causing considerably more speech degradation than encountered by the TBPE codec.

In general, most robust performance is achieved if the bit protection is carefully matched to the bit sensitivites, but the SEG-SNR and *CD* sensitivity measures portrayed in Fig. 11 often contradict. Therefore, we combine the two measures to give a sensitivity figure S, representing the average sensitivity of a particular bit. The bits must be first ordered both according to their SEG-SNR and *CD* degradations given in Figs. 11*a* and 11*b*, respectively, to derive their 'grade of prominance' with 1 representing the highest and 63 the lowest sensitivity. Observe that the highest *CD* degradation is caused by bit 6, which is the MSB of the second LSF in the speech frame, while the highest SEG-SNR degradation is due to bit 40 in the group of bits 37–43, representing the LTP delay. Furthermore, bit 6 is the seventh in terms of its SEG-SNR degradation, hence its sensitivity figure is $S = 1 + 7 = 8$, as seen in the first row of Table 2. On the other hand, the corruption of bit 40, the most sensitive in terms of SEG-SNR, results in a relatively low *CD* degradation, as it does not degrade the spectral envelope representation characterised by *CD*, but spoils the pitch periodicity and hence the spectral fine-structure. This bit is the 19th in terms of its SEG-SNR degradation, giving a sensitivity figure contribution of 19 plus 1 due to *CD* degradation, i.e. the combined sensitivity figure is $S = 20$, as shown by row 6 of Table 2. The combined sensitivity figures for all the LSFs and the first 27-bit subsegment are similarly summarised in ascending order in column 3 of Table 2, where column 2 represents the bit index in the first 63-bit segment of the 144-bit TBPE frame.

7 Combined system

Having selected and characterised the modulation, FEC coding and speech coding schemes most suited for the lightweight handheld portable phones for PCN, we now match the system elements to provide good speech quality. The system block diagram is depicted in Fig. 12. The bits of the TBPE speech encoder are mapped by the TBPE MAP circuit to the inputs of three different BCH encoders, *BCHE*/*C*1, /*C*2, /*C*3, which code the bits for channels *C*1, *C*2 and *C*3, respectively. The coded bit sequences are assembled in the ASM QAM block for modulation and transmission via the channel. After AGC and demodulation at the receiver the bitstream is disassembled in the DASM QAM block and BCH decoding of the three subchannels ensues. The speech bits are demapped by the TBPE DEMAP memory matrix to their original positions in the speech frame and TBPE decoding is performed.

We have shown that the probability of bit error is dependent on the transmitted phasor, and that the bits may be classified as belonging to one of three subchannels, *C*1, *C*2 or *C*3. If we have no prior knowledge of the nature of the data to be transmitted, e.g. whether it is encoded speech or computer data, then an appropriate strategy is to BCH code the data assigned to *C*1, *C*2 and *C*3 channels such that the error correcting power of the codes matches the ratios of the raw BERs. By coding the *C*1, *C*2 and *C*3 data with BCH(63, 57, 1), BCH(63, 51, 2) and BCH(63, 36, 5) we satisfy this criterion when the fast-fading tracking AGC is used and the channel SNR exceeds 25 dB. The number of data bits encoded per block by the three codecs is 144, and all codecs generate the same 63 bits per block.

However, for the TBPE codec with its bits having different error sensitivites as demonstrated by Fig. 11, we must select three BCH codecs, which together with the raw BERs of $C1$, $C2$ and $C3$ approximately match these bit error sensitivites. We will transmit on each BCH/64-QAM subchannel blocks of 63 bits, coding the 144 TBPE bits into 189 bits to yield a transmission rate of 189 bits per 30 ms = 6.3 Kbit/s, which at 6 bits per symbol gives 1.05 Kbaud. To this we must add a 10% channel sounding overhead i.e. $k = 10$ to facilitate the fade tracking AGC, to give 1.155 Kbaud, or 7.2 Kbit/s.

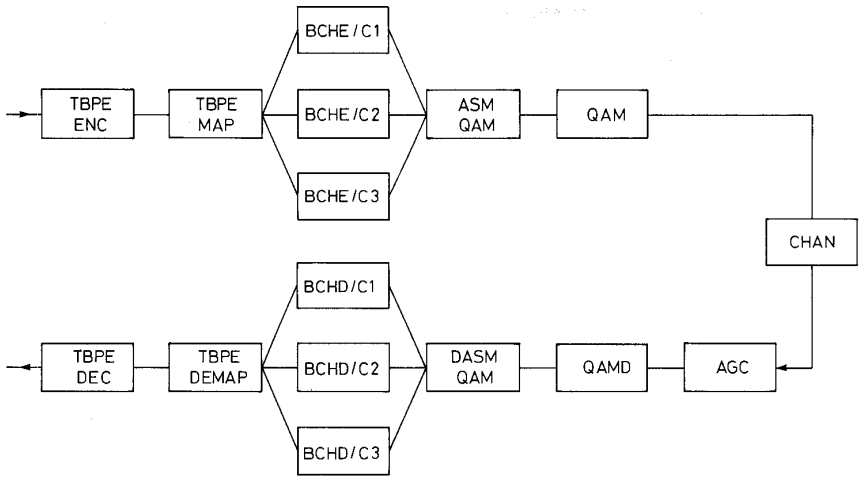

Fig. 12 *System block diagram*

We were tempted to operate the system with only two BCH codecs. Initially we eliminated the BCH coder for $C1$, allowing 63 bits to be mapped onto the 64-level QAM. BCH(63, 45, 3) and BCH(63, 36, 5) codes were used for $C2$ and $C3$, respectively. The most vulnerable TBPE bits were transmitted via $C1$, namely the 36 LSF bits and the MSBs of LTPD and LTPG. The 12 bits representing the subsegment excitations as well as the two grid position bits were fairly robust, and tolerated the higher BER of the least robust BCH/QAM subchannel. The rest of the bits were in the medium sensitivity category and were transferred via the $C2$ BCH/QAM subchannel. The performance was found to be dominated by the errors in the $C1$ subchannel, and for SNR < 35 dB the speech was somewhat blurred. Errors in $C2$ and $C3$ tended to occur in bursts which typically lasted for the complete 30 ms frame.

To eliminate the blurring we used BCH(63, 51, 2) and BCH(63, 30, 6) for subchannels $C1$ and $C2$, respectively, and discarded the BCH coder for $C3$. Although the most robust bits were transmitted via $C3$, the large number of them (63 per block) resulted in poor system performance.

Finally, we used BCH(63, 57, 1), BCH(63, 36, 5) and BCH(63, 51, 2) on subchannels $C1$, $C2$, $C3$, respectively. According to the codes chosen, 57, 36 and 61 bits can be transmitted via the $C1$, $C2$ and $C3$ subchannels, respectively. Those bits in the 144-bit frame with indices less than 37 represented the LSFs, and the remaining 108 bits were constituted by 28 + 26 + 28 + 26 bits describing the four subsegments. Therefore, selecting a bit with an index less than 37 for transmission via a specific QAM subchannel required the inclusion of one bit in that subchannel. As far as bits with higher indices are concerned, selecting, for example, the first one of a subsegment for a specific subchannel required the inclusion of the first bits of all four subchannels, as they had identical sensitivities. With these principles and Table 2 in mind, we finally constructed Table 3, describing the bits transmitted via the individual subchannels. Clearly, the FEC-coded bits 6, 9, 5, etc. of the 144-bit TBPE frame are sent via the $C1$ subchannel, bits 51, 78, 105, etc. through the $C2$, while bits 62, 89, 116, etc. via the appropriately protected $C3$ 64-QAM subchannel. Observe that the number of bits in each subchannel is adjusted to yield the same number of bits after FEC-coding. This bitmapping is carried out by the TBPE MAP block depicted in Fig. 12. The objective performance of our final arrangement is depicted in Fig. 13 for transmissions over Rayleigh fading channels, mobile speeds of 0 mile/h and 2 mile/h, and with and without diversity reception. When the mobile was stationary the transmissions were over an AWGN channel. Owing to the memorylessness of the AWGN channel its SEGSNR curve had a pronounced 'elbow' when the error correcting power of the BCH codes began to be frequently exceeded. When the AWGN channel SNR was

Table 3: Bit-allocation for *C1*, *C2* and *C3* subchannels

C1	*C2*	*C3*	*C1*	*C2*	*C3*
6	51	62	93	142	81
9	78	89	120	59	108
5	105	116	4	86	135
3	132	143	21	113	53
41	29	60	12	140	82
68	35	87	38	15	109
95	44	114	65		136
122	71	141	92		56
40	98	34	119		85
67	125	50	25		112
94	32	77	16		139
121	48	104	52		18
13	75	131	79		33
2	102	31	106		49
43	129	55	133		76
70	24	82	7		103
97	63	109	1		130
124	90	136	37		26
8	117	27	64		30
46	144	23	91		22
73	57	14	118		36
100	84	47	45		
127	111	74	72		
42	138	101	99		
69	10	128	126		
96	28	58	11		
123	19	85	20		
17	61	112			
39	88	139			
66	115	54			

below 22–24 dB, most of the BCH codewords were overloaded and the system performance was poor. Observe that when second-order diversity was used, the system achieved similarly favourable performance to that over

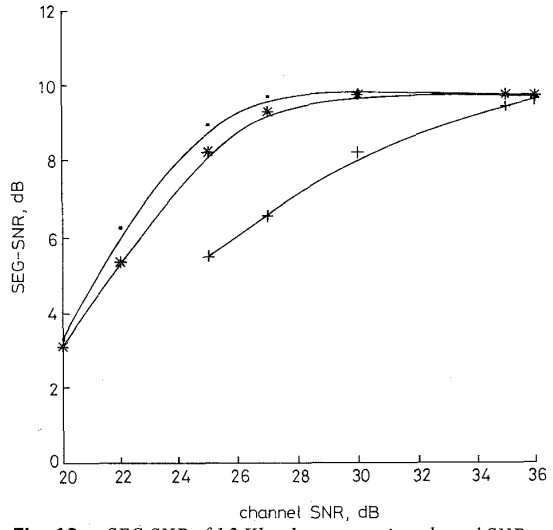

Fig. 13 *SEG-SNR of 1.2 Kbaud system against channel SNR*
—■— AWGN
—|— 2 mile/h, DIV = 1
—*— 2 mile/h, DIV = 2

the AWGN channel, and the SNR needed to be in excess of 26 dB to get communications speech quality.

8 Summary and conclusion

With the prerequisite of a microcellular environment, the deployment of 64-QAM in Rayleigh-fading channels has been investigated both by theory and simulation. A 4.8 Kbit/s TBPE speech codec was used providing good 'communications quality' speech at relatively low complexity, an informal subjective assessment, implying mean opinion scores in excess of $MOS = 3$. The encoded speech bits were mapped using selected BCH codes onto the 64-QAM subchannels and transmitted at less than 1.2 Kbaud. The speech quality was maintained for channel SNRs in excess of 26–28 dB for pedestrian mobiles walking at speeds between 0 mile/h and 4 mile/h.

9 References

1 IKURA, M., OHNO, K., YAMAO, Y., and ADACHI, F.: 'Field experiments on TDMA mobile radio transmissions'. Proceedings of IEEE Vehicular Technology 1991, Conference, St. Louis, USA, pp. 669–674
2 HANZO, L., STEELE, R., and FORTUNE, P.M.: 'A sub-band coding, BCH coding and 16-QAM system for mobile radio speech communications', *IEEE Trans.*, 1990, **VT-39,** (4), pp. 327–339
3 FORTUNE, P.M., HANZO, L., and STEELE, R.: 'Transmission of SBC speech via 16-level QAM over mobile radio channel'. GLOBCOM'88 proceedings, Florida, pp. 832–836
4 SALAMI, R., WONG, K.H.H., APPLEBY, D.G., and STEELE, R.: 'A robust transformed binary vector excited codec with embedded error correction coding'. IEE Colloquium, 9 October 1989, London, Digest 1989/112, pp. 5/1–5/6
5 HANZO, L., SALAMI, R., and STEELE, R.: 'A 2.1 KBd speech transmission system for Rayleigh-fading channels'. IEE Colloquium on speech Coding, 9 October 1989, London, Digest 1989/112, pp. 10/1–10/5
6 WONG, K.H.H., HANZO, L., and STEELE, R.: 'Channel coding for satellite mobile channels', *Int. J. Satell. Commun.*, 1989, **7,** (2), pp. 143–163
7 HANZO, L., WONG, K.H.H., and STEELE, R.: 'Efficient channel coding and interleaving schemes for mobile radio communications'. IEE Colloquium, London, 22 February 1989
8 WONG, K.H.J., HANZO, L., and STEELE, R.: 'A sub-band codec with embedded Reed–Solomon coding for mobile radio speech communications'. ICCS'88 Proceedings, Singapore, pp. 709–713
9 STEELE, R., TWELVES, D., and HANZO, L.: 'Effect of cochannel interference on handover in microcellular mobile radio', *Electron. Lett.*, 1989, **25,** (20), pp. 1329–1330
10 SALAMI, R.A., HANZO, L., and APPLEBY, D.: 'A computationally efficient CELP codec with stochastic vectorquantisation of LPC parameters'. URSI-ISSE'89 Proceedings, Erlangen, Germany, September 1989, pp. 140–143
11 KITAWAKI, N., HONDA, M., and ITOH, K.: 'Speech quality assessment methods for speech-coding systems', *IEEE Commun. Mag.*, Oct. 1984, **22,** (10), pp. 26–33
12 GRAY, A.H. Jr., and MARKEL, J.D.: 'Distance measures for speech processing', *IEEE Trans.*, 1976, **ASSP-24,** (5), pp. 380–391

10 Appendix: 64-QAM performance via Rayleigh-fading channels

In Reference 2 we derived the theory of 16-QAM for transmissions over Rayleigh-fading channels. We use a similar approach for 64-QAM, although the demodulation process is far more complex. Our assumption is that the channel fading is not frequency-selective, i.e. all frequency components of the transmitted signal suffer the same attenuation $\alpha(t)$ and phase shift $\Phi(t)$. We also suppose that since the channel is slowly fading $\alpha(t)$ is a constant for the duration of a signalling interval, although it has a Rayleigh probability density function (PDF). The phase shift $\Phi(t)$ of the received signal is uniformly distributed over $[-\pi, \pi]$.

Owing to Rayleigh-fading the attenuation $\alpha(t)$, written for convenience as α, causes the instantaneous SNR γ to be $\alpha^2 E/N_0$, i.e. γ changes from one signalling interval to another. We first find the average probability of error $P(\gamma)$ for a specific γ and then average it over the possible range of γ weighted by the PDF $f(\gamma)$ (i.e. the probability of occurrence) of that specific SNR γ, namely

$$P = \int_0^\infty P(\gamma) f(\gamma)\, d\gamma \tag{16}$$

For the Rayleigh distributed attenuation α the PDF of its transformed version $\gamma = \alpha^2 E/N_0$ has a Chi-square distribution [2]

$$f(\gamma) = \frac{1}{\Gamma} e^{-\gamma/\Gamma} \tag{17}$$

where the average SNR is

$$\Gamma = \langle\gamma\rangle = \left\langle \alpha^2 \frac{E}{N_0} \right\rangle = \langle\alpha^2\rangle \frac{E}{N_0} = 2\alpha_0 \frac{E}{N_0} \tag{18}$$

as α has a Rayleigh PDF of

$$f(\alpha) = \left(\frac{\alpha}{\alpha_0^2}\right) \exp\left(-\alpha^2/2\alpha_0^2\right) \tag{19}$$

The formula for the $C1$ BER can be obtained by substituting the Gaussian channel result of eqn. 11 into eqn. 16 along with $f(\gamma)$ in eqn. 17, namely

$$P_{C1}(\Gamma) = \frac{1}{4\Gamma} \int_0^\infty \left\{ Q\left[\sqrt{\frac{\gamma}{21}}\right] + Q\left[3\sqrt{\frac{\gamma}{21}}\right] + Q\left[5\sqrt{\frac{\gamma}{21}}\right] + Q\left[7\sqrt{\frac{\gamma}{21}}\right] \right\} e^{-\gamma/\Gamma}\, d\gamma \tag{20}$$

This simple derivation is achieved because the $C1$ decision boundaries constituted by the coordinate axis are unaltered by the fading. However, the probability of bit error for the $C2$ and $C3$ cannot be derived without considering the effects of fading on each phasor and decision boundary individually.

When calculating the probability of bit error for $C2$, we acknowledge that although the received phasors are attenuated by the instantaneous α value, the receiver is arranged to demodulate with reference to the expected value $2\alpha_0$. The effect of fading must be computed individually for each phasor. For P_6 the modified protection distance d_1 measured from the decision boundary $4\bar{\alpha}d$ is seen from Fig. 1 to be $d_1 = 4\bar{\alpha}d - 3\alpha d$. If the modified protection distance is overcome by noise, erroneous decisions occur. If the modified protection distance $d_1 < 0$, then in the absence of noise the decisions are consistently erroneous. In the presence of noise the phasors can be carried back into the error-free decision domain by sufficiently large negative noise samples. In both cases the error probability is equivalent to the noise samples exceeding the protection distance, irrespective of its actual value. In terms of the $Q[\ ]$ function we have

$$P_{e6}(\gamma) = Q\left[\left(\frac{4\bar{\alpha}}{\alpha} - 3\right)\sqrt{\frac{\gamma}{21}}\right] \tag{21}$$

For the phasor P_5 the modified protection distance from the $C2$ decision boundary $4\bar{\alpha}d$ is $d_1 = 4\bar{\alpha}d - \alpha d$. Observe that the effect of the instantaneous attenuation α is now less profound than for P_6, where it is multiplied by a factor of three. Using this d_1 value in the argument of the $Q[\ ]$ function gives

$$P_{e5}(\gamma) = Q\left[\left(\frac{4\bar{\alpha}}{\alpha} - 1\right)\sqrt{\frac{\gamma}{21}}\right] \tag{22}$$

The modified protection distance from the $C2$ decision boundary at $4\bar{\alpha}d$ for P_7 is seen from Fig. 1 to be $d_1 = 4\bar{\alpha}d - 5\alpha d$, which yields an error probability of

$$P_{e7}(\gamma) = Q\left[\left(\frac{4\bar{\alpha}}{\alpha} - 5\right)\sqrt{\frac{\gamma}{21}}\right] \tag{23}$$

The phasor P_8 has the highest distance from the coordinate axis, therefore it is profoundly effected by the instantaneous fading. It has an associated protection distance of $d_1 = 4\bar{\alpha}d - 7\alpha d$ which results in an error probability of

$$P_{e8}(\gamma) = Q\left[\left(\frac{4\bar{\alpha}}{\alpha} - 7\right)\sqrt{\frac{\gamma}{21}}\right] \tag{24}$$

The partial $C2$ error probabilities from eqns. 21–24 have to be substituted in eqn. 16 along with eqn. 17 to deliver the average $C2$ BER:

$$\begin{aligned} P_{C2}(\Gamma) = \frac{1}{4\Gamma}\Bigg\{ & \int_0^\infty Q\left[\left(\frac{4\bar{\alpha}}{\alpha} - 1\right)\sqrt{\frac{\gamma}{21}}\right] e^{-\gamma/\Gamma}\, d\gamma \\ & + \int_0^\infty Q\left[\left(\frac{4\bar{\alpha}}{\alpha} - 3\right)\sqrt{\frac{\gamma}{21}}\right] e^{-\gamma/\Gamma}\, d\gamma \\ & + \int_0^\infty Q\left[\left(\frac{4\bar{\alpha}}{\alpha} - 5\right)\sqrt{\frac{\gamma}{21}}\right] e^{-\gamma/\Gamma}\, d\gamma \\ & + \int_0^\infty Q\left[\left(\frac{4\bar{\alpha}}{\alpha} - 7\right)\sqrt{\frac{\gamma}{21}}\right] e^{-\gamma/\Gamma}\, d\gamma \Bigg\} \end{aligned} \tag{25}$$

The $C3$ subchannel performance is computed similarly, but for each phasor there are two modified protection distances, d_1 and d_2. For example, for the phasor P_6 we find $d_1 = 6\bar{\alpha}d - 3\alpha d$ and $d_2 = 3\alpha d - 2\bar{\alpha}d$, representing the distances from the $C3$ decision boundaries at $6\bar{\alpha}d$ and $2\bar{\alpha}d$, respectively. When exposed to AWGN, the decisions are erroneous on one hand, if the modified protection distance d_1 is exceeded by the noise samples. This holds for negative d_1 values as well. Erroneous decisions are also encountered, if the phasor P_6 is carried across the $C3$ decision boundary at $2\bar{\alpha}d$ by sufficiently large negative noise samples. This happens whenever the noise value resides below the level $-d_2$. Accordingly, the $C3$ bit error probability for P_6 is

$$P_{e6}(\gamma) = Q\left[\left(\frac{6\bar{\alpha}}{\alpha} - 3\right)\sqrt{\frac{\gamma}{21}}\right] + Q\left[\left(3 - \frac{2\bar{\alpha}}{\alpha}\right)\sqrt{\frac{\gamma}{21}}\right] \tag{26}$$

Considering the case of the phasor P_5 the modified protection distances are $d_1 = 2\bar{\alpha}d - \alpha d$ and $d_2 = 6\bar{\alpha}d - \alpha d$, respectively. Erroneous decisions are engendered if the protection distance d_1 is exceeded by noise, but noise samples larger than d_2 carry the phasors into another error-free decision domain. Whence the error probability is

$$P_{e5}(\gamma) = Q\left[\left(\frac{2\bar{\alpha}}{\alpha} - 1\right)\sqrt{\frac{\gamma}{21}}\right] - Q\left[\left(\frac{6\bar{\alpha}}{\alpha} - 1\right)\sqrt{\frac{\gamma}{21}}\right] \tag{27}$$

When the phasor P_7 is transmitted the situation is characterised by the distances $d_1 = 6\bar{\alpha}d - 5\alpha d$ and $d_2 = 5\alpha d - 2\bar{\alpha}d$, and hence

$$\begin{aligned} P_{e7}(\gamma) = & Q\left[\left(\frac{6\bar{\alpha}}{\alpha} - 5\right)\sqrt{\frac{\gamma}{21}}\right] \\ & + Q\left[\left(5 - \frac{2\bar{\alpha}}{\alpha} - 1\right)\sqrt{\frac{\gamma}{21}}\right] \end{aligned} \tag{28}$$

Finally, for the phasor P_8 we find $d_1 = 7\alpha d - 6\bar{\alpha}d$ and $d_2 = 7\alpha d - 2\bar{\alpha}d$, where errors are caused by noise samples below the level $-d_1$. Should, however, the noise vector fall below $-d_2$, the phasors are switched to another error-free decision domain across the decision boundary at $2\bar{\alpha}d$, therefore

$$P_{e8}(\gamma) = Q\left[\left(7 - \frac{6\bar{\alpha}}{\alpha}\right)\sqrt{\frac{\gamma}{21}}\right] - Q\left[\left(7 - \frac{2\bar{\alpha}}{\alpha}\right)\sqrt{\frac{\gamma}{21}}\right] \tag{29}$$

Assume again that random sequences are sent, i.e. the probability of each phasor $P_1, \ldots, P_{64}$ occurring is identical, and further, exploit the symmetry of the signal constellation. On substituting eqns. 26–29, along with eqn. 17, into eqn. 16 we obtain the average $C3$ bit error probability as a function of the average SNR Γ, namely

$$\begin{aligned} P_{C3}(\Gamma) = \frac{1}{4\Gamma}\Bigg\{ & \int_0^\infty \left[Q\left[\left(\frac{6\bar{\alpha}}{\alpha} - 3\right)\sqrt{\frac{\gamma}{21}}\right] + Q\left[\left(3 - \frac{2\bar{\alpha}}{\alpha}\right)\sqrt{\frac{\gamma}{21}}\right]\right] e^{-\gamma/\Gamma}\, d\gamma \\ & + \int_0^\infty \left[Q\left[\left(\frac{2\bar{\alpha}}{\alpha} - 1\right)\sqrt{\frac{\gamma}{21}}\right] - Q\left[\left(\frac{6\bar{\alpha}}{\alpha} - 1\right)\sqrt{\frac{\gamma}{21}}\right]\right] e^{-\gamma/\Gamma}\, d\gamma \\ & + \int_0^\infty \left[Q\left[\left(\frac{6\bar{\alpha}}{\alpha} - 5\right)\sqrt{\frac{\gamma}{21}}\right] + Q\left[\left(5 - \frac{2\bar{\alpha}}{\alpha} - 1\right)\sqrt{\frac{\gamma}{21}}\right]\right] e^{-\gamma/\Gamma}\, d\gamma \\ & + \int_0^\infty \left[Q\left[\left(7 - \frac{6\bar{\alpha}}{\alpha}\right)\sqrt{\frac{\gamma}{21}}\right] - Q\left[\left(7 - \frac{2\bar{\alpha}}{\alpha}\right)\sqrt{\frac{\gamma}{21}}\right]\right] e^{-\gamma/\Gamma}\, d\gamma \Bigg\} \end{aligned} \tag{30}$$

In summary, the $C1$, $C2$ and $C3$ subchannel performances over Rayleigh-fading channels are given by eqns. 20, 25 and 30 respectively.